

# Wide-Bandwidth Coaxial PWB Transmission Line Probe

N. G. Paulter, R. H. Palm, and D. D. Barry

**Abstract**—The design, fabrication, and test of a wide-bandwidth (3-dB attenuation bandwidth  $\geq 30$  GHz), 50  $\Omega$ , passive coaxial probe for the electrical characterization of printed wiring board (PWB) transmission lines is described. The probe can make thousands of repeated contacts, using spring-loaded interconnects, without affecting probe performance. The probe contains an internal mechanism for dissipating static charge on the signal line of the PWB transmission line and is long enough (approximately 10 cm) to act as a transfer standard for characteristic impedance testing, as per the time-domain reflectometry test method described in IPC TM 2.5.5.7.

**Index Terms**—Bandwidth, characteristic impedance, coaxial probe, electrical testing, hollow glass spheres, printed wiring board (PWB), probe, static dissipation, step response.

## I. INTRODUCTION

CONDUCTING lines on printed wiring boards (PWBs) are used to interconnect passive and active devices and provide input/output connections. For high-performance (high-speed, high-frequency, high data rate) boards, these conducting lines behave more as transmission lines than as simple conductors and must be modeled and measured accordingly. Three important performance characteristics of a transmission line are its characteristic impedance, its propagation delay, and its propagation loss. These performance characteristics are important for several reasons: transmission line design verification, material and fabrication process qualification, quality control, and supplier qualification. The measurement of these characteristics are typically performed using time-domain reflectometry (TDR) because of the ease of use of the instruments, the ready interpretation of the data, and the relatively low cost to purchase and maintain TDR tools compared to frequency domain tools. The probe described herein for the characterization of high-performance printed wiring board transmission lines has three characteristics that make it very suitable for this task: its construction is a 50- $\Omega$  airline so that it

Manuscript received July 6, 2007; revised November 27, 2007. This work was recommended for publication by Associate Editor A. Shapiro upon evaluation of the reviewers comments.

N. G. Paulter was with the Quantum Electrical Metrology Division, Electronics and Electrical Engineering Laboratory, Technology Administration, Department of Commerce, Gaithersburg, MD 20899 USA. He is now with the Office of Law Enforcement Standards, Gaithersburg, MD 20899 USA.

R. H. Palm is with the Quantum Electrical Metrology Division, Electronics and Electrical Engineering Laboratory, Technology Administration, Department of Commerce, Gaithersburg, MD 20899 USA.

D. D. Barry is with Fabrication Technology Division, Manufacturing Engineering Laboratory, Technology Administration, Department of Commerce, Gaithersburg, MD 20899 USA.

Color versions of one or more of the figures in this paper are available online at <http://ieeexplore.ieee.org>.

Digital Object Identifier 10.1109/TEPM.2008.919354

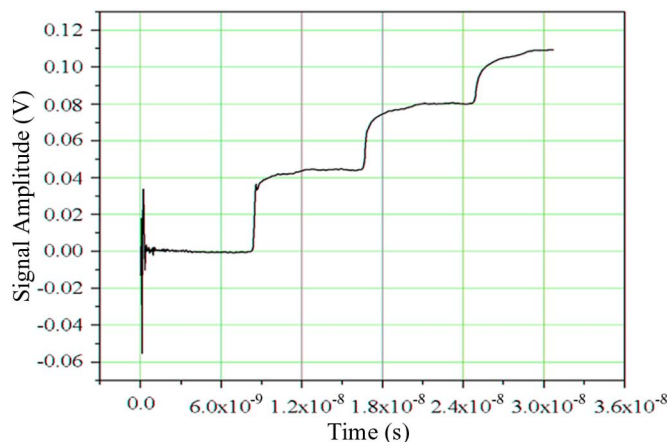


Fig. 1. Example of a TDR waveform showing multiple reflections.

can be used as an impedance transfer standard, its bandwidth is 30 GHz or greater making it useful for characterization of present and future designs, and it has an internal structure for dissipating static on the signal line thus protecting the TDR instrumentation from damage by electrostatic discharge.

Detail on the TDR method can be found elsewhere [2], but a very brief description is given here. In TDR, a pulse, the incident pulse, is launched from the TDR head into a device under test (DUT). In this case described herein, the DUT will be a transmission line. The incident pulse is sampled within the TDR head as it travels toward the TDR input/output connector; this gives the reference or incident part of the TDR waveform. After the incident pulse leaves the TDR head, any impedance discontinuities that the incident pulse encounters will result in a reflection of a portion of the incident pulse; this is the reflected pulse. The amplitude of the reflected pulse is dependent on the difference between the TDR and DUT impedances. The reflected pulse returns to the TDR head and is superposed with the incident pulse at the sampler, which is inside the TDR head, to provide the TDR waveform. The reflected and incident pulses are delayed with respect to each other, and this delay is dependent on the pulse propagation velocity in and the length of the transmission line. An example of a TDR waveform is shown in Fig. 1.

To determine the electrical characteristics of the transmission line under test (TLUT), and to do this in a cost effective and timely way to a large set of TLUTs, requires that the contacting device make easily breakable and repeatable contact to the TLUT. This is both a mechanical and electrical requirement. The probe must also launch signals onto and receive signals from a planar transmission line. The contacting device should have a nominal impedance of 50  $\Omega$  because this is the most commonly used impedance in high-frequency/high-speed

circuits and instruments. The contacting device must also possess sufficient bandwidth to minimally distort (that is, cause distortion that is within or less than the expected measurement uncertainty) the signals launched onto and extracted from the TLUT. The contacting device described herein is a coaxial probe that meets these requirements and provides other features that can improve overall measurement system measurement performance and reduce measurement uncertainty (see list below).

Probe contacts	>100 000, no observable change in signal amplitude or transient characteristics for repeated use of up to 100 000 cycles [3].
Characteristic impedance	50.0 $\Omega$ (see Section II-A).
Uncertainty	$\leq \pm 0.5 \Omega$ (see Section II-A).
-3-dB bandwidth	$\geq 30$ GHz (see Section II-B).
Internal static protection	No other devices needed.

Although the probe that will be described can be modified to accommodate differential transmission lines, the focus here will be on application to single-ended transmission lines.

## II. PROBE CHARACTERIZATION

The probe was characterized using TDR measurements. The primary performance characteristics of the probe that were measured with TDR are its characteristic impedance,  $Z_{\text{prb, meas}}$ , and its 3-dB attenuation bandwidth.

### A. Characteristic Impedance, Measured, $Z_{\text{prb, meas}}$

The value of  $Z_{\text{prb, meas}}$  is determined from TDR measurement using the ratio of the amplitude  $V_r$  of the pulse reflected at the probe/TDR interface to the amplitude  $V_i$  of the incident pulse. The ratio of these pulse amplitudes is the reflection coefficient  $\rho$

$$\rho = \frac{V_r}{V_i} \quad (1)$$

where

$$V_r = \text{level}(s_{2, \text{prb}}) - \text{level}(s_{1, \text{prb}}) \quad (2)$$

and  $\text{level}(s_{2, \text{prb}})$  and  $\text{level}(s_{1, \text{prb}})$  are the amplitude levels (see [4]) of the high and low states for the reflected pulse, and

$$V_i = \text{level}(s_{2, \text{ref}}) - \text{level}(s_{1, \text{ref}}) \quad (3)$$

where  $\text{level}(s_{2, \text{ref}})$  and  $\text{level}(s_{1, \text{ref}})$  are the amplitude levels of the high and low states for the incident pulse.  $\rho$  is relative to the characteristic impedance  $Z_{\text{ref}}$  of the reference air line impedance, which is  $50 \Omega \pm 0.3 \Omega$ . Because of how the TDR measurement method was implemented for this particular situation (the reference is an open-terminated air line, the probe is not terminated, and no changes in timebase or gain settings were made between reference and transmission line measurements)

$$\text{level}(s_{1, \text{ref}}) = \text{level}(s_{1, \text{prb}}). \quad (4)$$

TABLE I  
VARIABLES FOR THE COMPUTATION OF THE EXPANDED UNCERTAINTY OF  $Z_{\text{prb, meas}}$ , WHERE  $Z_{\text{prb, meas}}$  IS COMPUTED FROM THE TDR-MEASURED STATE LEVELS

variable	partial derivative	uncertainty
$\text{level}(s_{1, \text{prb}})$ (250 mV)	$\frac{-2}{\text{level}(s_{2, \text{ref}}) - \text{level}(s_{2, \text{prb}})} Z_{\text{ref}}$	$\sqrt{\sigma_{\text{noise}}^2 + \sigma_{\text{repeat}}^2}$ ( $< 200 \mu\text{V}$ )
$\text{level}(s_{2, \text{prb}})$ (255 mV)	$2 \frac{\text{level}(s_{2, \text{ref}}) - \text{level}(s_{1, \text{prb}})}{[\text{level}(s_{2, \text{ref}}) - \text{level}(s_{2, \text{prb}})]^2} Z_{\text{ref}}$	$\sqrt{\sigma_{\text{noise}}^2 + \sigma_{\text{repeat}}^2}$ ( $< 200 \mu\text{V}$ )
$\text{level}(s_{2, \text{ref}})$ (0 mV)	$2 \frac{\text{level}(s_{1, \text{prb}}) - \text{level}(s_{2, \text{prb}})}{[\text{level}(s_{2, \text{ref}}) - \text{level}(s_{2, \text{prb}})]^2} Z_{\text{ref}}$	$\sqrt{\sigma_{\text{noise}}^2 + \sigma_{\text{repeat}}^2}$ ( $< 200 \mu\text{V}$ )
$Z_{\text{ref}}$ (50 $\Omega$ )	$\frac{\text{level}(s_{2, \text{prb}}) + \text{level}(s_{2, \text{ref}}) - 2\text{level}(s_{1, \text{prb}})}{\text{level}(s_{2, \text{ref}}) - \text{level}(s_{2, \text{prb}})}$	0.3 $\Omega$

Therefore,  $\rho$  becomes

$$\rho = \frac{\text{level}(s_{2, \text{prb}}) - \text{level}(s_{1, \text{prb}})}{\text{level}(s_{2, \text{ref}}) - \text{level}(s_{1, \text{prb}})}. \quad (5)$$

The characteristic impedance,  $Z_{\text{prb, meas}}$ , of the probe is computed from  $\rho$  and  $Z_{\text{ref}}$  to give

$$Z_{\text{prb, meas}} = \frac{1 + \rho}{1 - \rho} Z_{\text{ref}}. \quad (6)$$

Rewriting  $Z_{\text{prb, meas}}$  in terms of the measured state levels gives

$$Z_{\text{prb}} = \frac{\text{level}(s_{2, \text{prb}}) + \text{level}(s_{2, \text{ref}}) - 2\text{level}(s_{1, \text{prb}})}{\text{level}(s_{2, \text{ref}}) - \text{level}(s_{2, \text{prb}})} Z_{\text{ref}}. \quad (7)$$

The uncertainty in  $Z_{\text{prb, meas}}$  is found from

$$u_{Z_{\text{prb}}} = \sqrt{\sum_{i=1}^4 \left( \frac{\partial Z_{\text{prb}}}{\partial \alpha_i} \sigma_i \right)^2} \quad (8)$$

where  $\alpha_i$  represents the four variables from which  $Z_{\text{prb, meas}}$  is computed. The partial derivatives are shown in Table I. Test transmission lines were used to verify the design formula (see Section III-B1). All designs tried were coaxial with either air or hollow glass spheres for the dielectric. The hollow glass spheres, however, were not used in the final probe design because of the increased uncertainty in the probe's characteristic impedance when using these spheres (discussed in Section III-B1). The hollow glass spheres were examined because we felt the spheres would provide better alignment of the center conductor within the outer conductor than the dielectric washers (located at the ends) alone. This was shown not to be the case. However, the results of computing the uncertainty in the characteristic impedance using a dielectric other than air is edifying and, so, is included in this manuscript.

Using 1.106 for the value of  $\langle \epsilon'_{h, \text{gs}} \rangle$  (see Appendix 1),  $d_o = 1.396 \text{ mm} \pm 2.9 \times 10^{-3} \text{ mm}$ , and  $d_i = 3.356 \text{ mm} \pm 5 \times 10^{-3} \text{ mm}$ , the theoretical (predicted) impedance value  $Z_{\text{prb}}$  for the transmission line using hollow glass spheres is  $50.01 \Omega \pm$

1.050  $\Omega$ . Transmission lines using the spheres were then fabricated to have the dimensions shown above and their characteristic impedances determined using TDR methods. The value of  $Z_{prb,meas}$  computed from the TDR data is  $50.04 \Omega \pm 0.30 \Omega$ , where the dominant contributor to uncertainty was that from the reference airline. Using air alone as the dielectric for the probe, the appropriate transmission line dimensions are:  $d_o = 1.396 \text{ mm} \pm 2.9 \times 10^{-3} \text{ mm}$  and  $d_i = 3.216 \text{ mm} \pm 5 \times 10^{-3} \text{ mm}$ , which gives a theoretical impedance of  $49.99 \Omega \pm 0.14 \Omega$  and a TDR-measured value of  $49.80 \Omega \pm 0.30 \Omega$ .

### B. Bandwidth

The 3-dB attenuation bandwidth of the probe is obtained by deconvolving the reference step (the incident step) from the reflected step. First however, the reference step has to be corrected for signal content that occurs independent of termination and is common in the acquired TDR waveforms. To correct the reference step, the common signal contribution  $v_{com}[t]$  is found first:

$$v_{com}[t] = \frac{v_{refl,sh}[t] - v_{refl,op}[t]}{2} \quad (9)$$

where  $v_{refl,sh}[t]$  is the waveform obtained by connecting a short-circuit termination to the TDR,  $v_{refl,op}[t]$  is the waveform obtained by connecting an open-circuit termination to the TDR, and “[t]” is the discrete time index.  $v_{com}[t]$  can then be subtracted from either  $v_{refl,sh}[t]$  or  $v_{refl,op}[t]$  to yield the corrected reference waveform,  $v_{inc}[t]$ . The reflected step  $v_{ref}[t]$  is obtained by replacing the short-circuit termination with the probe and acquiring another waveform without changing the time-base delay or sensitivity (time per division) settings of the TDR. These time-domain waveforms are processed [5] and then transformed into complex spectra,  $V_{inc}[f]$  and  $V_{ref}[f]$  (where “[f]” is a discrete frequency index), using Fourier transforms. These spectra provide the signal transfer function  $\Gamma[f]$  of the probe

$$\Gamma[f] = \sqrt{\frac{V_{ref}[f]}{V_{inc}[f]}}. \quad (10)$$

The square root is used to get the one-way signal transfer function (see Fig. 2). The 3-dB attenuation bandwidth (the frequency at which the signal power is one-half that at  $f = 0$ ) is greater than 30 GHz.

## III. DESIGN OF THE PROBE

The probe design comprises three general physical regions: the connectorized region, the uniform transmission line region, and the contact region. The probe is required to launch signals onto and receive signals from a planar transmission line. Consequently, the probe was designed to be passive with a characteristic impedance that matches the impedance of the test instrumentation.

### A. Connectorized Region

The connectorized region provides the electrical interface between the TDR and other electronic instruments. To reduce reflections caused by the interface between the probe and other electronics, the probe is designed so that the inside diameter  $d_i$

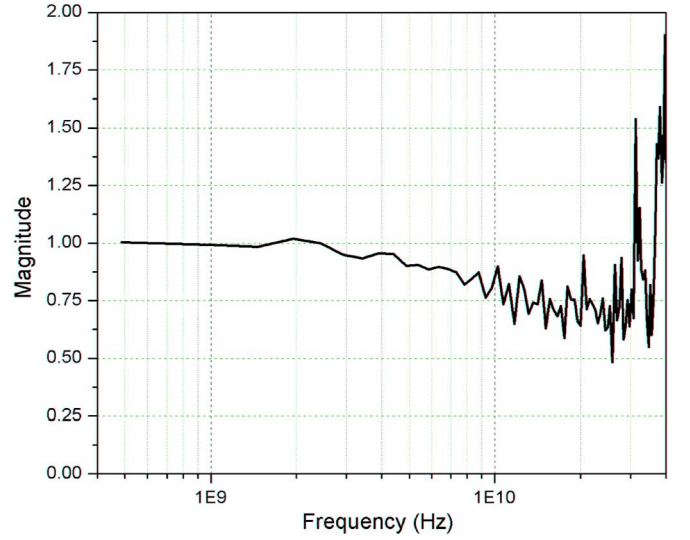


Fig. 2. Transfer function of probe. The oscillatory nature of the plot after 30 GHz is an artifact of measurement noise.

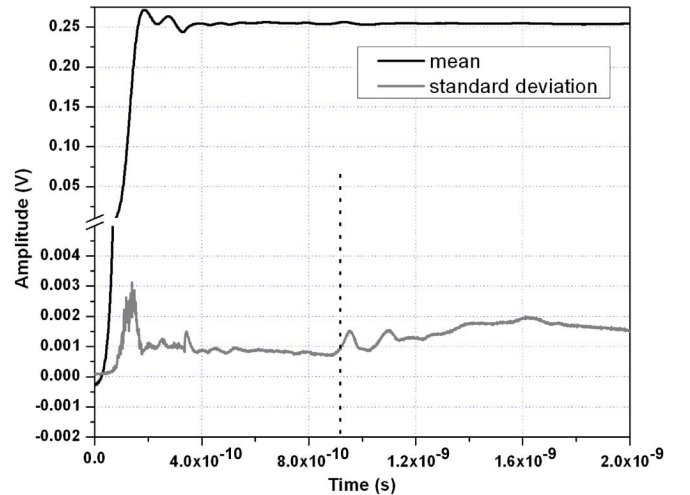


Fig. 3. Mean TDR waveform showing interface between TDR head and probe. Also shown is the standard deviation of the set of waveforms used (see Section III-A). The dotted vertical indicates the nominal “location” of the probe/TDR interface.

of the outer (or ground or reference) conductor is uniform over its full length. The outside diameter  $d_o$  of the inner (or signal) conductor is uniform in diameter up to where the outer conductor ends (see Section IV-A) to mate to the female connector of another device, such as a TDR head. The reduction in  $d_o$  is accomplished by making the last 2 mm of the tip a smaller diameter than the rest of the inner conductor, as is done in most (if not all) high-frequency ( $\sim$  3-dB bandwidth  $>$  20 GHz) miniaturized coaxial connectors for mating to a female connector. Six probes were manufactured and their electrical interface with the TDR measured. Fig. 3 shows the mean and standard deviation for this set of probes. Four measurements were taken for each probe, where the probes were disconnected and reconnected to the TDR for each measurement. The dotted vertical line in Fig. 3 represents the approximate “location” of the probe/TDR interface in the TDR waveform. The mean and standard deviation

TABLE II

VALUES USED TO COMPUTE  $Z_{\text{prb, meas}}$  (THE MEASURED VALUE) AND  $Z_{\text{prb}}$  (THE THEORETICAL, OR PREDICTED, VALUE) FOR THE TEST TRANSMISSION LINES. THE VALUES IN BRACKETS ARE THE UNCERTAINTIES ASSOCIATED WITH THAT PARAMETER. THE INFORMATION PROVIDED IN THIS TABLE WAS USED TO TEST THE ACCURACY OF PREDICTING AND MANUFACTURING THE PROBES. THE RADII SHOWN BELOW WERE NOT USED IN THE DESIGN OF THE FINAL PROBE

$d_o$ (mm)	1.089 {1.3x10 <sup>-3</sup> }		1.396 {2.9x10 <sup>-3</sup> }		2.392 {2.6x10 <sup>-3</sup> }	
dielectric	air	hgs	air	hgs	air	hgs
$level(s_{2,ref})$ (mV)	5.6 {0.14}	5.6 {0.14}	5.6 {0.15}	5.6 {0.15}	5.7 {0.13}	5.7 {0.13}
$level(s_{1,prb})$ (mV)	-240.8 {0.12}	-240.8 {0.12}	-240.8 {0.26}	-240.8 {0.26}	-240.0 {0.11}	-240.0 {0.11}
$level(s_{2,prb})$ (mV)	-202.0 {0.08}	-207.8 {1.10}	-229.7 {.40}	-234.6 {0.54}	-335.4 {1.98}	-341.1 {2.09}
$Z_{\text{prb, meas}}(\Omega)$	68.69 {0.42}	65.46 {0.72}	54.71 {0.39}	52.58 {0.41}	22.26 {0.44}	21.08 {0.45}
$\epsilon'_{\text{hgs}}$	1.106 {0.028}		1.087 {0.023}		1.124 {0.025}	
value of $\langle \epsilon'_{\text{hgs}} \rangle$ used in transmission line section design: $1.106 \pm 0.047$						
value of $d_i$ used for all test transmission lines: $3.454 \text{ mm} \pm 5 \times 10^{-3} \text{ mm}$						
$Z_{\text{prb}}(\Omega)$	69.21 {0.11}	65.81 {1.40}	54.32 {0.15}	51.65 {1.11}	22.03 {0.11}	20.95 {0.46}

plots to the right of this line represent measurement repeatability, connect/disconnect reproducibility, and probe manufacture reproducibility. The standard deviation to the left of this line represents measurement repeatability. Some of the oscillatory nature in the standard deviation is due to drifts in delay between subsequent waveforms. Although the delay component corresponding to integer multiples of the sampling interval (0.5 ps for the waveforms shown in Fig. 3) was removed prior to computation of the standard deviation, the residual noninteger delay was not removed. The average precorrected delay was nominally 67.1 ps with a nominal range of 6.1 ps and standard deviation of 1.6 ps.

### B. Transmission Line Region

The primary design considerations for the transmission line region are its characteristic impedance and length. To act as a reference impedance, the transmission line region has to be accurately machined and the electromagnetic properties of the materials used accurately known. Furthermore, the line has to be long enough to separate reflections in the TDR waveform. The characteristic impedance of the probes, as determined from TDR data prior to TDR correction (see Section II-A), is  $49.8 \Omega \pm 0.3 \Omega$  (for  $d_o = 1.396 \text{ mm} \pm 2.9 \times 10^{-3} \text{ mm}$ ,  $d_i = 3.216 \text{ mm} \pm 5 \times 10^{-3} \text{ mm}$ , and with air as the dielectric).

*Design Using Physical Dimensions and Material Properties:* The transmission line is a uniform coaxial transmission line. The

dielectric used in the transmission line was either air or hollow glass spheres, both with a 0.5-mm-thick dielectric washer on the probe tip end to hold the center conductor in place. The center conductor is held in place at the connector end by a female-to-female adapter.

The length of the transmission line section is limited by machining considerations (see Section IV). The characteristic impedance  $Z_{\text{prb}}$  of the transmission line section assuming ideal conductors and lossless dielectrics (the ideal case, see Section III-B2) can be computed using [6]

$$Z_{\text{prb}} = \sqrt{\frac{\mu}{\epsilon_0}} \frac{1}{2\pi \sqrt{\langle \epsilon'_{\text{hgs}} \rangle}} \ln \left( \frac{d_i}{d_o} \right) \quad (11)$$

where  $\langle \epsilon'_{\text{hgs}} \rangle$  is the average of the real part of the permittivity of the hollow glass spheres (see Appendix 1),  $\mu$  is the magnetic permeability of the conductors,  $\epsilon_0$  is the permittivity of free space,  $d_o$  is the outside diameter of the inner conductor of the transmission line, and  $d_i$  is the inside diameter of the outer conductor of the transmission line. The design of the transmission line region is dependent on the value of  $\langle \epsilon'_{\text{hgs}} \rangle$ , which is unknown. To determine this value, several test transmission lines were made and tested (see Appendix 1). For transmission lines made using air as the dielectric,  $\langle \epsilon'_{\text{hgs}} \rangle$  is replaced by 1. Table II shows that the uncertainty in  $\langle \epsilon'_{\text{hgs}} \rangle$  causes a significant increase in  $u_{Z_{\text{prb}}}$  compared to the case where the dielectric is air.

TABLE III  
VARIABLES FOR THE COMPUTATION OF THE EXPANDED UNCERTAINTY OF  $Z_{\text{prb}}$ , WHERE  $Z_{\text{prb}}$  IS COMPUTED FROM THE ANALYTIC FORMULA (11)

variable	partial derivative	uncertainty
$\epsilon'_{hgs}$	$-\sqrt{\frac{\mu}{\epsilon_0}} \frac{1}{4\pi} \ln\left(\frac{d_i}{d_o}\right) \frac{1}{\epsilon'^{3/2}_{hgs}}$	see Table 2
$d_o$	$\sqrt{\frac{\mu}{\epsilon_0}} \frac{1}{\sqrt{\epsilon'_{hgs}}} \frac{1}{2\pi} \frac{1}{d_o}$	$< 3 \mu\text{m}$
$d_i$	$-\sqrt{\frac{\mu}{\epsilon_0}} \frac{1}{\epsilon'_{hgs}} \frac{1}{2\pi} \frac{1}{d_i}$	$< 3 \mu\text{m}$

*Analysis of Transmission Line Section:* The characteristic impedance of any uniform continuous transmission line is given by (see, for example, [6])

$$Z_{\text{gen}} = \sqrt{\frac{R(\omega) + j\omega L(\omega)}{G(\omega) + j\omega C(\omega)}} \quad (12)$$

where  $R$ ,  $L$ ,  $G$ , and  $C$  are the resistance, inductance, conductance, and capacitance, all per unit length, of the transmission line, and  $\omega$  is the angular frequency.  $R$ ,  $L$ ,  $G$ , and  $C$  are shown as a function of  $\omega$  because of the effects of materials properties (frequency-dependent penetration of current into finite-conductivity conductors and frequency-dependent dielectric properties of insulators). For the dielectrics used here, the material is either air or primarily air; therefore,  $G \approx 0$ . Also,  $R$  is small for the conductors (copper, aluminum, and brass) and frequencies ( $< 20$  GHz) used here. Consequently, (12) can be approximated using a Taylor series expansion with  $G \approx 0$  and for small  $R$  ( $R < 5 \Omega$ , as determined using a field solver)

$$Z_{\text{gen}} \approx \sqrt{\frac{L_0}{C_0}} \left( 1 + \frac{R^2}{8\omega^2 L^2} - j \frac{R}{2\omega L} \right) \quad (13)$$

where  $L_0$  and  $C_0$  are the frequency-independent inductance and capacitance per unit length of the transmission line section. The value of  $L$  and  $L_0$  is about  $1.8 \times 10^{-7}$  Hz and  $R \leq 5 \Omega$  for the geometries and materials used in the probe. Consequently, for frequencies greater than 1 GHz (as is the case for the study described herein), the magnitude of  $Z_{\text{gen}}$  is approximately  $1.0001 Z_0$ , where

$$Z_0 = \sqrt{\frac{L_0}{C_0}}. \quad (14)$$

Because  $Z_0$  is real and independent of frequency over the frequency range of interest, (14), the ideal formula for a transmission line is a valid approximation of (13). Since (11) is the formula for the ideal coaxial line, (11) is a valid design formula for the characteristic impedance of the probes we have developed.

*Comparison of Measured and Predicted Characteristic Impedance:* In Appendix 1, measurements are described to determine  $\langle \epsilon'_{hgs} \rangle$ . These measurements were also used to determine if any systematic measurement errors caused a deviation of the measurement-based characteristic impedance

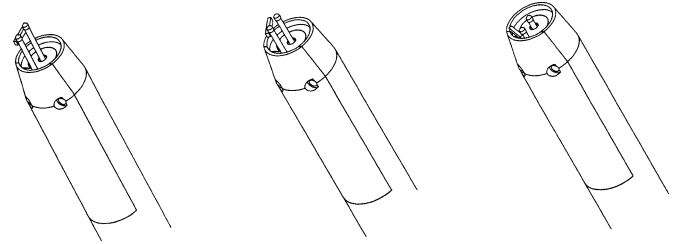


Fig. 4. Figures showing action of SDE. On the left, interconnects are fully extended and the SDE shunts the signal contact to the ground contact. The middle figure shows the contacts partially compressed. On the right, the contacts are fully compressed and the SDE is maximally rotated away from the signal contact.

values from the predicted (theoretical) values. The uncertainty values and coefficients for the parameters in (11) are shown in Table III. The measurement-based values  $Z_{\text{prb, meas}}$  shown in Table II are computed using (7). The relationship between the values of  $Z_{\text{prb}}$  (the theoretical or predicted values based on material properties and geometries) and  $Z_{\text{prb, meas}}$  for the air dielectric (see Table II) indicate that there are no obvious systematic measurement errors (as would be indicated by the average difference between  $Z_{\text{prb}}$  and  $Z_{\text{prb, meas}}$ , which is  $-0.033 \Omega \pm 0.400 \Omega$ ).

### C. Contact Region

The contact region is the most important part of the probe for maintaining high bandwidth. This part must also sustain repeated contacts (many thousands) without affecting the performance of the probe. To provide the repeated contact requirement, the probe uses spring-loaded interconnects for both the ground and signal contact [3]. To maintain the high bandwidth at the contact region of the probe, the probe is designed so that when the spring-loaded interconnects are fully depressed, the heads of these interconnects are recessed into the body of the probe (see Fig. 4 and Section IV).

Within the contact region, a mechanism for shunting any static electricity on the signal line of the TLUT to ground is also provided. The operation of this static dissipation element (SDE) is shown in Fig. 4. Shown in Figs. 5 and 6 are the TDR waveforms for the probe in full contact (interconnect fully depressed) with a dielectric, to represent an open, and a brass block, to represent a short. Four measurements were taken for

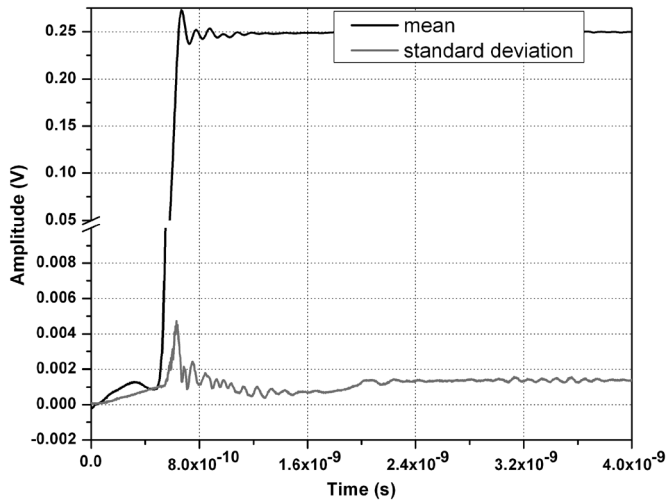


Fig. 5. Mean TDR waveform with probe tip compressed and in contact with a dielectric, thus emulating an open. Also shown is the standard deviation of the set of waveforms used (see Section III-C).

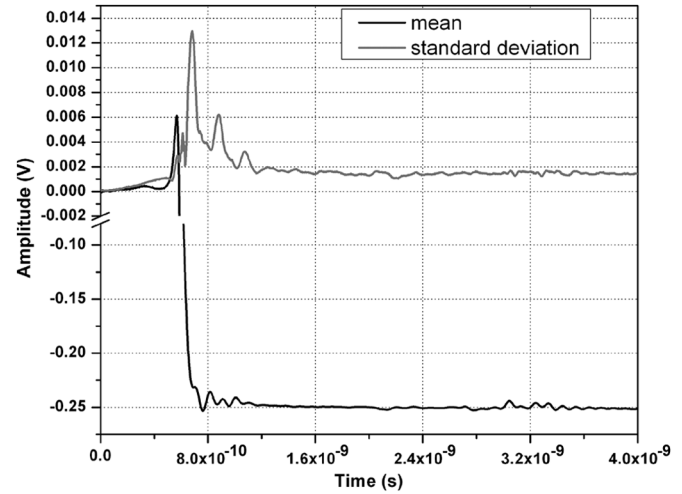


Fig. 6. Mean TDR waveform with probe tip compressed and in contact with a brass block, thus emulating a short. Also shown is the standard deviation of the set of waveforms used (see Section III-C).

each of the six probes, where the probes were disconnected and reconnected to the TDR for each measurement. Consequently, the mean and standard deviation shown in Figs. 5 and 6 represent measurement repeatability, connect/disconnect reproducibility, and probe manufacture reproducibility. The effect of the SDE on the TDR waveform is included in these waveforms. Some of the oscillatory nature in the standard deviations is due to drift in delay between subsequent waveforms. Although that delay corresponding to integer multiples of the sampling interval (1.0 ps for the waveforms shown in Figs. 5 and 6) was removed prior to computation of the standard deviation, the residual noninteger delay was not removed. The average precorrected delay for the open-circuit case was nominally 610 ps with a nominal range of 14 ps and standard deviation of 3.7 ps and, for the short-circuit case, was nominally 640 ps with a nominal range of 24 ps and standard deviation of 5.4 ps. The probes were used manually and, consequently, a greater variation is observed in Figs. 5 and 6 than in Fig. 3. Moreover, the short-circuit case was much more sensitive to positioning than the open-circuit case, which is exhibited by the differences in the standard deviation waveforms of Figs. 5 and 6.

The spectrum of a representative impulse response for a probe is shown in Fig. 2. The dc resistance of the SDE was measured to be  $0.063 \Omega \pm 0.015 \Omega$ . The probe was operated hundreds of times with no observable change in the electrical performance of the SDE.

#### IV. PROBE FABRICATION

The probe (see Fig. 7) consists of several parts (see parts list in Table IV). The inner and outer conductors, the SDE, and the ground interconnect holding elements are fabricated at NIST; the other components can be purchased from an appropriate manufacturer.

##### A. Inner (Signal) Conductor

The considerations for the inner conductor are its electrical conductivity, machinability, and assembly tolerance (that

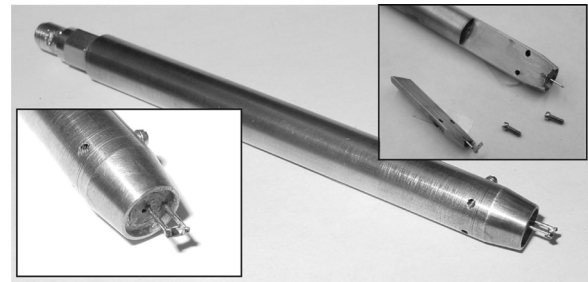


Fig. 7. Photograph of the probe. The inset, bottom left, shows probe tip with SDE-interconnect fully extended. The SDE is making electrical contact to the signal line. The inset, top right, shows the disassembled probe tip. The SDE-interconnect is contained within the ground interconnect holder.

is, whether its dimensions will be affected by the assembly process). Most metals are easily machined, but the inner conductor must be machined without introducing bends, kinks, perforations, or any other mechanical flaws that would impact the electrical performance of the probe. It was decided therefore, that a rod of appropriate diameter  $d_o$  would be obtained from a manufacturer and  $d_i$  would be determined based on this value of  $d_o$  and the value of the permittivity of the dielectric used. Using a  $d_o$  fixed by a rod manufacturer reduces machining requirements and minimizes introduction of mechanical flaws. This requirement, plus that for a high electrical conductivity, a relative permeability of 1, low cost, and the availability of rod with  $d_o \approx 1.5$  mm limits the materials to aluminum, brass, and copper. Aluminum was not used because the native oxide of aluminum may cause a poor electrical contact between the spring-loaded interconnect and the inner conductor and between the inner conductor and the mating surface of any connecting device. Brass was selected because, for the diameters used, was easier to machine than copper.

The center conductor is a small diameter rod with a reduced diameter point on one end and a long coaxial hole on the other end (see Fig. 8). This piece was produced on a conventional lathe using a fixture to capture the brass rod for the purpose of

TABLE IV  
PARTS USED IN THE FABRICATION OF THE PROBE

Part	Description
signal contact	spring-loaded interconnect: 0.790 mm dia. x 31.59 long x 6.35 mm travel x 105 g force
ground contact	spring-loaded interconnect: 0.790 mm dia. x 31.59 long x 6.35 mm travel x 105 g force x 90° rotation
SMA connector	size to fit “.141” diameter semi-rigid cable
SMA adapter	female-to-female “barrel”
dielectric washer	0.5 mm thick x 0.89 mm I.D. x 4.78 mm O.D, $\epsilon_r \leq 4$
outer conductor	machined copper, see Fig. 8
inner conductor	machined brass, see Fig. 7
ground contact holder	machined brass, see Fig. 9
static dissipation element	brass, 0.51mm thick x 0.762 mm wide x 2.54 mm long
screws	0-80, fillister head, 3 mm long

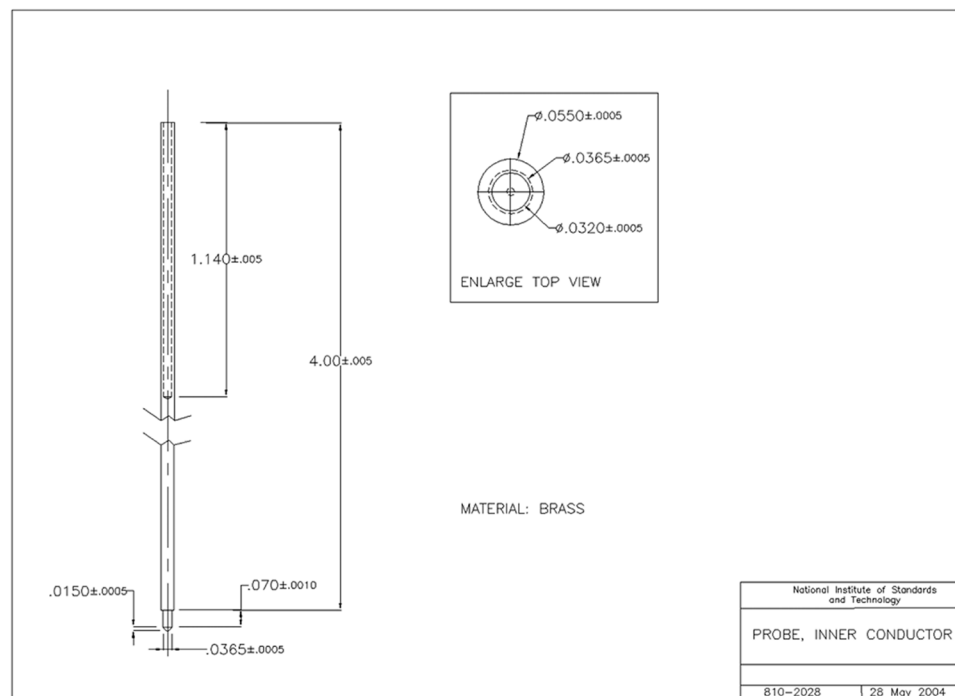


Fig. 8. Mechanical drawing of inner conductor.

alignment during machining and to help prevent the side wall from rupture during the drilling process.

### B. Outer (Ground) Conductor

The considerations for the outer conductor (see Fig. 9), including the ground interconnect holder (see Fig. 10), are the same as for the inner conductor; therefore, the material requirements were restricted to brass and copper. Brass was not used because of its lower electrical conductivity compared to copper.

Conventional machining practices are adequate to produce these two copper pieces. The diameter and length of both were cut on a lathe, and most holes were drilled and tapped on a

milling machine. The coaxial through-hole on the outer conductor (see Fig. 9) and the hole for holding the spring-loaded interconnect on the ground interconnect holder (see Fig. 10) were produced using wire electrical discharge machining (EDM). EDM was used to produce the deep through-hole in the outer conductor for a number of reasons: accuracy, lack of cutting force, ease of setup, and the fact that we had it available. The through-hole could have been produced on conventional machinery, but the risk of failure became much more likely because of the aspect ratio of the hole, the tight tolerance (12.7  $\mu\text{m}$  [0.0005 in]) on the diameter, concentricity to the outside diameter of the outer conductor, and the cylindricity required for

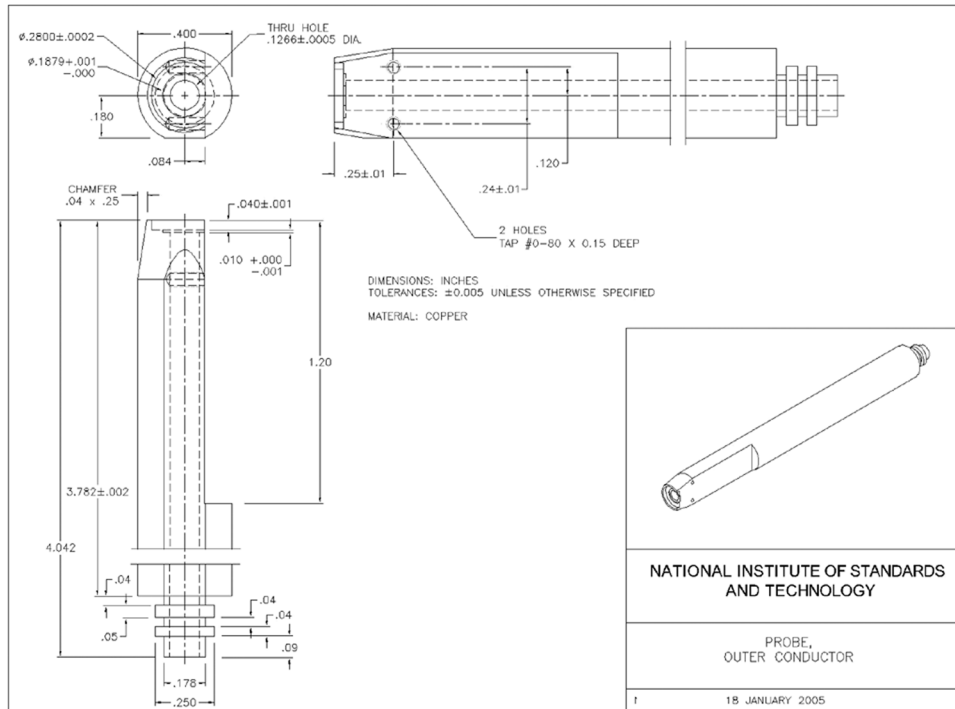


Fig. 9. Mechanical drawing of outer conductor.

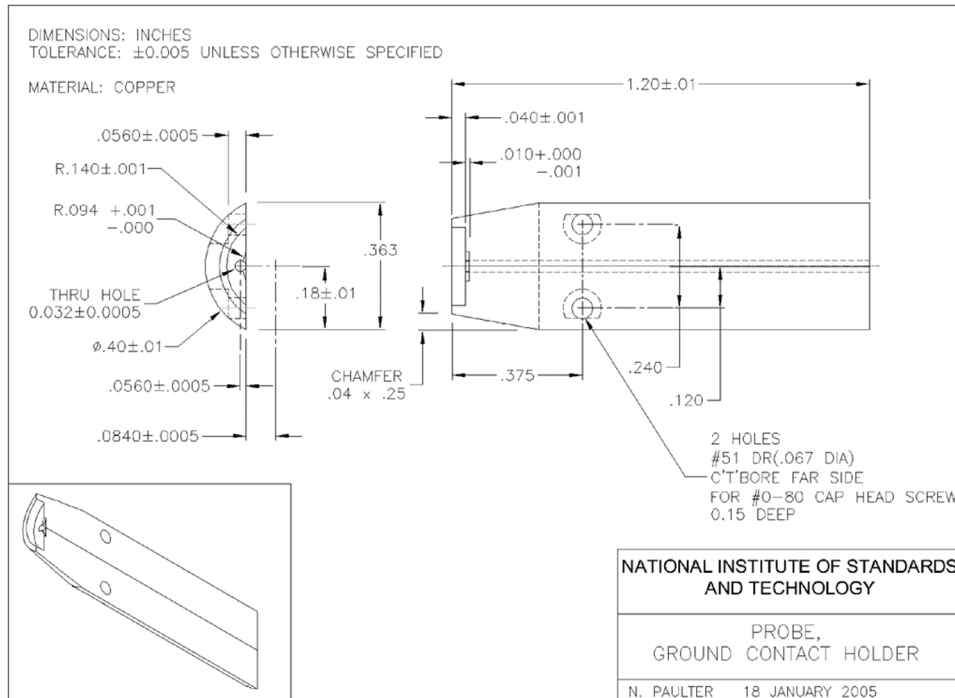


Fig. 10. Mechanical drawing of ground interconnect (contact) holder.

the probe assembly to function within the engineered specifications.

The SDE is attached to a rotating spring-loaded interconnect. The SDE-interconnect assembly is positioned in the body of the probe so that the SDE makes contact with the center conductor when the SDE-interconnect is fully extended. Since the SDE is flexible, this position ensures that electrical contact is made between the ground and signal line until the SDE-interconnect

is depressed. As the SDE-interconnect is depressed, it rotates 90°, thus breaking contact with the signal line.

### C. Probe Assembly

The following are the steps in the assembly of the probe:

- 1) Solder the connector nut attachment piece (manufacturer dependent) to the body.
- 2) Attached the connector nut to the probe.

- 3) Fix the position of the inner conductor to the outer conductor at the connector end using a female-to-female adapter, which becomes a part of the probe.
- 4) Carefully place the dielectric washer between the inner and outer conductors at the tip end of the probe. When the dielectric washer is properly positioned, glue it in place, and let the glue dry.
- 5) Insert the spring-loaded interconnect into the inner conductor of the probe.
- 6) Solder the SDE to the spring-loaded interconnect of the ground contact. The SDE should be attached as close as possible to the head of the spring-load interconnect but not to this head.
- 7) Insert the ground contact spring-loaded interconnect into the ground contact holder.
- 8) Attach the ground contact holder to the probe body using appropriate screws.

## V. SUMMARY

The coaxial PWB transmission line probe was designed, fabricated, and tested. Testing shows the probe meets the desired electrical characteristics: 3-dB attenuation bandwidth  $\geq 30$  GHz, characteristic impedance of nominally  $50 \Omega$ , and probe measurement repeatability was within measurement uncertainty for at least 100 000 contacts (cycles of probe compression and release). The integral static protection provided a ground shunt resistance of less than  $0.1 \Omega$  and eliminates the need for ancillary signal-line-to-ground switches, which adds cost and reduces the bandwidth of the measurement system. The probe can be mounted directly to a TDR head, thus eliminating the need for additional cabling and connectors, which affect signal integrity. The probe is long enough that the transmission line part of the probe can act as a reference impedance if manufactured accurately. Unique parts of the probe can be made with conventional manufacturing tools. The design fits typical requirements for factory-floor operation: it can be used as a hand-held device (with training) or on an automated machine, and the breakable parts, the spring-loaded interconnects, are inexpensive and easily replaced.

## APPENDIX A

### II. ESTIMATION OF $\langle \varepsilon'_{hgs} \rangle$

Three different test transmission line sections were fabricated and tested for the purpose of determining the approximate value of  $\langle \varepsilon'_{hgs} \rangle$  necessary for the final probe design. Table II shows the measured voltage values, the computed characteristic impedances, and  $\varepsilon'_{hgs}$  values for each test transmission line.  $\varepsilon'_{hgs}$  for each test transmission line is computed using

$$\varepsilon'_{hgs} = \left( \frac{Z_{air}}{Z_{hgs}} \right)^2. \quad (15)$$

The corresponding uncertainty in  $\varepsilon'_{hgs}$  is computed using

$$u_{\varepsilon} = 2 \frac{Z_{air}}{Z_{hgs}} \sqrt{\frac{1}{Z_{hgs}^2} u_{Z_{air}}^2 + \left( \frac{Z_{air}}{Z_{hgs}} \right)^2 u_{Z_{hgs}}^2}. \quad (16)$$

The value of the permittivity of the hollow glass spheres used to design the transmission line region is actually the average  $\langle \varepsilon'_{hgs} \rangle$  of the three  $\varepsilon'_{hgs}$  values, one taken from each of the test transmission lines. The uncertainty for this average value is given by

$$u_{\langle \varepsilon'_{hgs} \rangle} = \sqrt{u_{\varepsilon_{1.089 \text{ mm}}}^2 + u_{\varepsilon_{1.396 \text{ mm}}}^2 + u_{\varepsilon_{2.392 \text{ mm}}}^2 + \sigma_{\text{set}}^2} \quad (17)$$

where  $u_{\varepsilon_{1.089 \text{ mm}}}$ ,  $u_{\varepsilon_{1.396 \text{ mm}}}$ , and  $u_{\varepsilon_{2.392 \text{ mm}}}$  are the uncertainties in  $\varepsilon'_{hgs}$  computed for each test transmission line and  $\sigma_{\text{set}}$  is the variation in this set of the computed values of  $\varepsilon'_{hgs}$ .

## REFERENCES

- [1] "Characteristic impedance of lines on printed boards by TDR," IPC, Northbrook, IL, IPC-TM-650 Test Methods, 2.5.5.7 Rev. A, Mar. 2004 [Online]. Available: [http://www.ipc.org/4.0\\_Knowledge/4.1\\_Standards/test/2-5-5-7a.pdf](http://www.ipc.org/4.0_Knowledge/4.1_Standards/test/2-5-5-7a.pdf)
- [2] "Design guide for high-speed controlled impedance circuit boards," IPC, Northbrook, IL, IPC-2141A, Mar. 2004.
- [3] N. G. Paulter and R. H. Palm, "A wide bandwidth printed wiring board transmission line probe," in *IPC Printed Circuits Expo '99*, Long Beach, CA, Mar. 14–18, 1999, pp. S19-4-1–S19-4-4.
- [4] *IEEE Standard on Transitions, Pulses, and Related Waveforms*, IEEE Standard 181-2003, The IEEE, New York, Jul. 2003.
- [5] N. G. Paulter, "Reducing the effects of record truncation discontinuities in waveform reconstructions," *IEEE Trans. Instrum. Meas.*, vol. 42, no. 3, pp. 695–700, Jun. 1993.
- [6] S. Ramo, J. R. Whinnery, and T. Van Duzer, *Fields and Waves in Communication Electronics*, 2nd ed. New York: Wiley, 1984.

**N. G. Paulter** received the M.S. degree in chemistry from the University of New Mexico, Albuquerque, in 1988 and the M.S. degree in electrical engineering from the University of Colorado, Boulder, in 1990.

He was with Los Alamos National Laboratory, Los Alamos, NM, from 1980 to 1989 and was involved in the study of fast electrical phenomena and in the development of high-speed photoconductors for use as ultrafast light detectors and electrical sampling gates. In 1989, he joined the National Institute of Standards and Technology (NIST), Boulder, CO, to develop transient pulse measurement techniques and analysis. He is currently a Program Manager at NIST, Gaithersburg, MD, with programs in millimeter-wave concealed weapon detection, RF through-barrier sensing, and imaging metrology.

**R. H. Palm**, photograph and biography not available at the time of publication.

**D. D. Barry** has been a Prototype Machinist/Tool Maker for 27 years. He joined NIST in November of 1989 as a Journeyman Machinist/Instrument Maker specializing in electrical discharge machining (EDM).